

Bis-Metal Complexes of Doubly N-Confused Dioxohexaphyrins as Potential Near Infrared-II Photoacoustic Dyes

Keito Shimomura, Hiroto Kai, Yuma Nakamura, Yongseok Hong, Shigeki Mori, Koji Miki, Kouichi Ohe, Yusuke Notsuka, Yoshihisa Yamaoka, Masatoshi Ishida, Dongho Kim, and Hiroyuki Furuta

J. Am. Chem. Soc., **Just Accepted Manuscript** • Publication Date (Web): 09 Feb 2020

Downloaded from pubs.acs.org on February 9, 2020

Just Accepted

“Just Accepted” manuscripts have been peer-reviewed and accepted for publication. They are posted online prior to technical editing, formatting for publication and author proofing. The American Chemical Society provides “Just Accepted” as a service to the research community to expedite the dissemination of scientific material as soon as possible after acceptance. “Just Accepted” manuscripts appear in full in PDF format accompanied by an HTML abstract. “Just Accepted” manuscripts have been fully peer reviewed, but should not be considered the official version of record. They are citable by the Digital Object Identifier (DOI®). “Just Accepted” is an optional service offered to authors. Therefore, the “Just Accepted” Web site may not include all articles that will be published in the journal. After a manuscript is technically edited and formatted, it will be removed from the “Just Accepted” Web site and published as an ASAP article. Note that technical editing may introduce minor changes to the manuscript text and/or graphics which could affect content, and all legal disclaimers and ethical guidelines that apply to the journal pertain. ACS cannot be held responsible for errors or consequences arising from the use of information contained in these “Just Accepted” manuscripts.

Bis-Metal Complexes of Doubly N-Confused Dioxohexaphyrins as Potential Near Infrared-II Photoacoustic Dyes

Keito Shimomura,[†] Hiroto Kai,[†] Yuma Nakamura,[†] Yongseok Hong,[‡] Shigeki Mori,[§] Koji Miki,[⊥] Kouichi Ohe,[⊥] Yusuke Notsuka,[⊥] Yoshihisa Yamaoka,[⊥] Masatoshi Ishida,^{*,†} Dongho Kim,^{*,‡} and Hiroyuki Furuta^{*,†}

[†]Department of Chemistry and Biochemistry, Graduate School of Engineering, and Center for Molecular Systems, Kyushu University, Fukuoka 819-0395, Japan

[‡]Department of Chemistry, Yonsei University, Seoul 03722, Korea

[§]Advanced Research Support Center, Ehime University, Matsuyama 790-8577, Japan

[⊥]Department of Energy and Hydrocarbon Chemistry, Graduate School of Engineering, Kyoto University, Kyoto 615-8510, Japan

[⊥]Department of Advanced Technology Fusion, Graduate School of Science and Engineering, Saga University, Saga 840-8502, Japan

ABSTRACT: We investigated the detailed photophysical properties of a series of bis-metal (Zn and Cu) dioxohexaphyrin complexes as potential second near-infrared (NIR-II)-light responsive dyes. A *cisoid*-configured 28 π -electron-conjugated dioxohexaphyrin analog (**c-3a**) containing two peculiar “confused pyrrole” moieties in the framework is identified as a reduced isomer derivative of a *transoid* 26 π -dioxohexaphyrin (**t-2a**). The symmetry-altered structure of **c-3a** affords a heteroleptic inner environment within the *NNNN/NNOO* donor core, which imparts its highly flexible electronic features and nonplanar geometry. The macrocycle **c-3a** can be transformed into the corresponding 26 π -electron congener (**c-2a**) having a coplanar rectangular structure by unique solvent-mediated redox reactivity. Furthermore, upon metal complexation, saddle-distorted bis-metal complexes (**c-M₂-2a**) were formed as the 26 π -conjugated structural isomer of the *trans*-dioxohexaphyrin species (i.e., **t-M₂-2a**). These isoelectronic dioxohexaphyrins demonstrate precise geometry-dependent photophysical properties. Broad tailing NIR-II absorption, weak emissive character, and rapid-decay of the S₁ state are observed for **c-Zn₂-2a**. In contrast, the coplanar **t-M₂-2a** exhibits efficient photoacoustic response upon laser excitation with NIR-II light ($\lambda > 1000$ nm). To the best of our knowledge, this is the first example of an expanded porphyrin-based photoacoustic contrast agent responsive to NIR-II light.

INTRODUCTION

Expanded porphyrins consisting of more than five pyrrole rings have recently emerged as an important class of near-infrared (NIR) dye chromophores owing to their large and flexible π -conjugated scaffolds. Accordingly, they offer new possibilities in the development of optical materials for use in fields ranging from light-harvesting to sensing and therapeutic applications.^{1–5} Their distinct photophysical properties are exclusively conformation-dependent based on Hückel and Möbius topological aromaticity.⁶ Furthermore, their unique ability to coordinate various metal ions leads to well-defined π -conjugated structures in solution, aiding the design of novel NIR dyes for biological applications.⁷

Meso-aryl-substituted hexaphyrin (**4**) has been extensively studied owing to their conformation-dependent optical features, including cation-responsive NIR emission,^{8,9} NIR-light excited photothermal/photodynamic properties,^{10,11} and NIR-light chiral recognition ability (Figure 1).^{12–16}

Absorption in the far NIR region beyond 1000 nm (termed as the second near-infrared region, or NIR-II) is an attractive property for photoacoustic imaging (PAI) technologies.^{17–19} In PAI, incident light photons are absorbed by a dye agent and converted into heat. There-

upon, broadband ultrasonic emission is generated in the biological tissue by thermal expansion, which can be detected by an acoustic transducer. Absorption in the NIR-II window provides clear advantages over that in the conventional NIR-I window (700–1000 nm) for deeper tissue imaging as it provides higher maximum permissible exposures (MPEs)²⁰ (e.g., λ_{ex} at 800 nm is ~ 300 mW/cm² and at 1064 nm is ~ 1000 mW/cm² per laser pulse) and reduced light scattering^{21,22} in the tissues. The PA properties of small molecular NIR dyes, such as indocyanine green (ICG),²³ aza-BODIPYs,^{24,25} bis(benzothiadiazole)-derivatives (e.g., NIRb-14),^{26,27} benzi-phthalocyanine,²⁸ and hybrid cyclopyrrole analog (C-P1P4F1)^{29,30} have been extensively examined. Distorted phosphorus-phthalocyanine (P-Pc) showing strong absorption around 1000 nm has been proven to be an efficient PA agent for deep *in-vitro* imaging to depths of several centimeters upon excitation using a Nd:YAG laser (1064 nm).^{31,32} Such research is of fundamental interest as a means to explore the structure-property relationships of NIR-II absorbers as potential PA contrast agents, which are currently in high demand for biomedical applications.

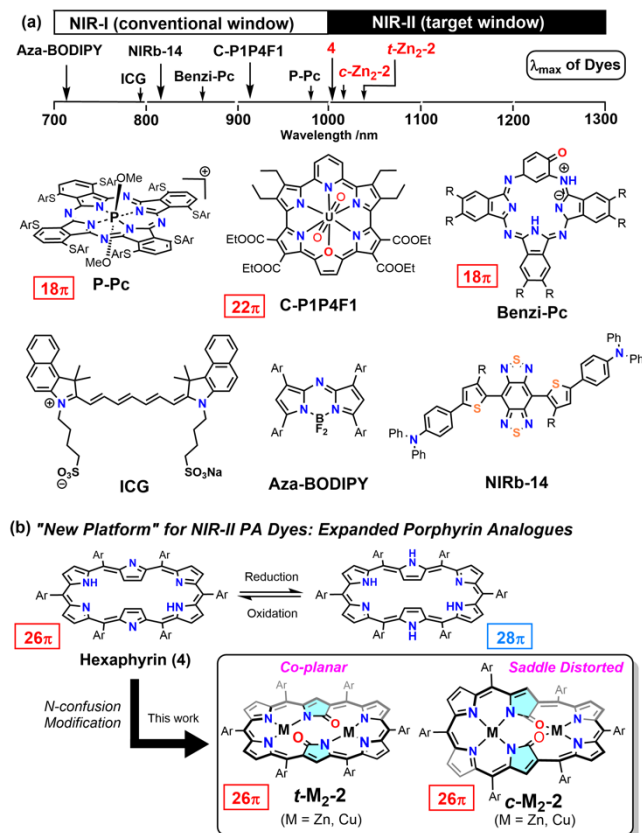
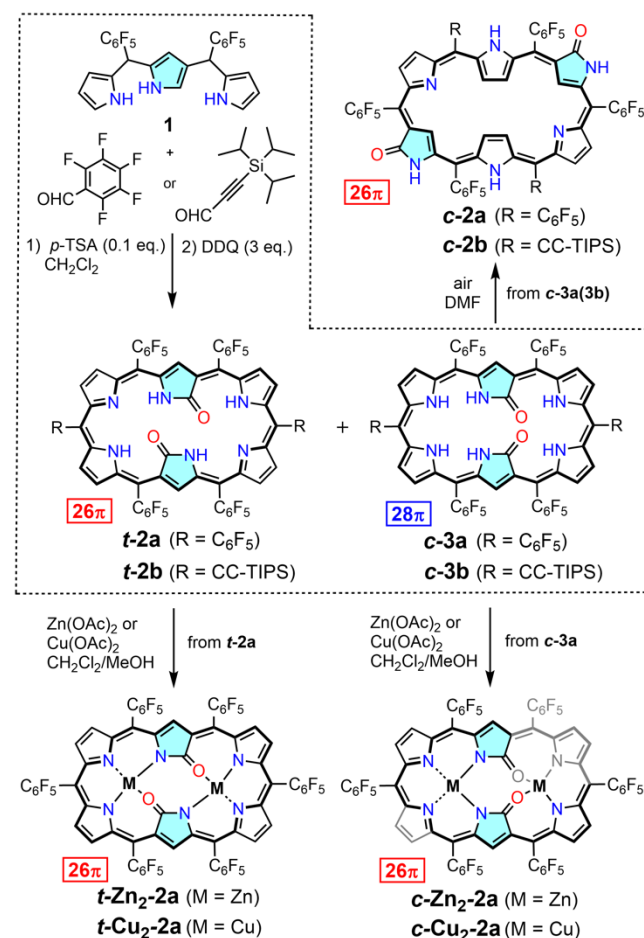


Figure 1. (a) Excitation (absorption) energy-structure relationship for several representative NIR-PA dyes and some expanded porphyrins. (b) Redox-interconvertible hexaphyrins containing doubly N-confused congeners with different molecular symmetries can serve as functional and tunable NIR-II PA dyes.

To create well-defined NIR-II dyes, chemical modification of the hexapyrrolic core by a N-confusion approach as a means to tailor the inner coordination sphere is a viable approach.^{33,34} The implementation of confused pyrrole rings (highlighted in sky-blue in Figure 1) connected at the α - and β' -positions between the *meso*-carbon atoms of the parent hexaphyrin skeleton allows a predominantly planar rectangular conformation because of the hydrogen-bond network between the inward-facing nitrogen atoms and carbonyl groups of the pyrrole rings.^{35,36} Thus, the doubly N-confused dioxohexaphyrin **t-2** is rigidified upon accommodation of a metal atom at either symmetric NNNO sphere with the highly planar 26π -circuit (**t-M₂-2**; Figure 1b). Analogously to planar π -systems, the rearrangement of confused pyrroles as a pair to a *cisoid* configuration upon metal coordination at the NNNN–NNOO core (**c-M₂-2**; Figure 1b) would provide a new prototype three-dimensional saddle-distorted hexaphyrin isomer.^{37,38} However, such complexes have yet to be observed. Nevertheless, knowledge of this phenomenon can provide insight into the effect of saddle distortion on fundamental photophysical properties. Accordingly, works related to saddle-distorted tetrapyrrolic systems have revealed their intriguing properties, such as the relatively high Lewis acidity of the central metal ion, relatively low redox potential, rapid decay of excited states, and weaker aromaticity.³⁹ However, the effect of such distortion on the nonradiative decay of laterally π -extended porphyrins (i.e., hexaphyrins) is still not fully understood.

In this study, we investigated the photophysical properties of dioxohexaphyrins, including the first structurally characterized *cisoid*-analog (**c-3**), along with the symmetrical *transoid*-congener (**t-2**; Scheme 1). The resulting *cisoid* 28π -electron derivative is converted to the corresponding Hückel 26π -conjugated form through aerobic oxidation in basic solvents such as dimethylformamide (DMF) as well as upon bis-metalation. In fact, the resulting 26π -conjugated *cisoid* dioxohexaphyrins (**c-2** and **c-M₂-2**) are considered to be isomeric species of *transoid*-derivatives with different core geometries. The alteration of molecular symmetry in the *cis*- and *trans*-homologs plays a vital role in their photophysical and PA properties. To the best of our knowledge, the PA properties of hexaphyrin-related macrocycles have not been previously reported. In this study, the bis-metal complexes of dioxohexaphyrins exhibit superior PA spectral features responsive to NIR-II light.



Scheme 1. Synthetic Route to Dioxohexaphyrins **t-2**, **c-2**, and **c-3**, and their Bis-Metal Complexes **t-M₂-2** and **c-M₂-2**

RESULTS AND DISCUSSION

Synthesis and Characterization of Nonaromatic Dioxohexaphyrin c-3. Previously, we reported that the conventional acid-catalyzed [3+3]-condensation of a N-confused tripyrrane (**1**) and pentafluorobenzaldehyde in CH_2Cl_2 , followed by 2,3-dichloro-5,6-dicyano-1,4-benzoquinone (DDQ) oxidation yields *transoid* 26π -conjugated doubly N-confused dioxohexaphyrin **t-2a** as the major product along with the 28π -conjugated dioxo-congener having

nonaromatic character as a minor product (Scheme 1).^{37,38} Currently, we have not yet fully characterized the structure and properties of the latter species. The synthesis of dioxohexaphyrin **c-3a** using the modified protocol was revisited in this study. Short-term exposure (ca. 2 h) to the oxidant DDQ and careful purification led to the isolation of **c-3a** as a major product (Scheme 1). Due to the highly polar nature of the product, a careful column purification procedure was needed. This involved i) passing through a short alumina column pad to eliminate the tarry polymers, and ii) purification by silica gel column chromatography to collect the brown-colored fraction containing the hexaphyrin derivatives (ca. 10% yield).

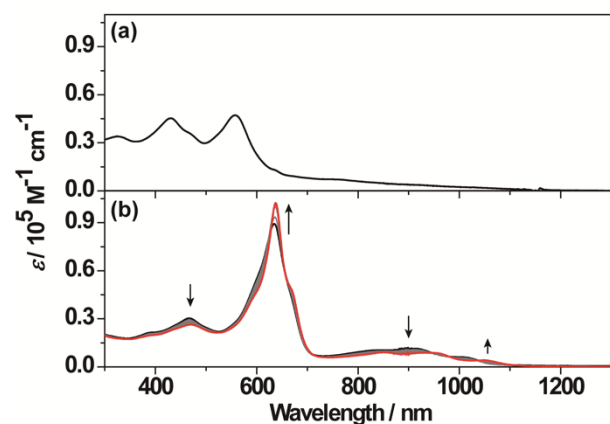


Figure 2. (a) UV-Vis-NIR absorption spectrum of **c-3a** in CH_2Cl_2 and (b) its absorption spectrum changes upon standing in DMF under aerobic conditions. The final spectrum (obtained after 48 h) is shown in red.

Analysis of the product **c-3a** using NMR, UV-Vis-NIR spectroscopy, and high-resolution mass spectrometry indicates a 28π nonaromatic electronic structure with *cisoid*-geometry (see Supporting Information). In the mass spectrum of **c-3a**, the M^+ peak observed at $m/z = 1494.0908$ (1494.0856 calcd for $\text{C}_{66}\text{H}_{16}\text{N}_6\text{O}_2\text{F}_{30}$) is two mass units larger than the parent peak of **t-2a**. The UV-Vis-NIR absorption spectrum of **c-3a** in CH_2Cl_2 presents a broad and poorly defined feature (Figure 2a). The ^1H NMR spectrum reveals five sets of β -pyrrolic protons in the typical sp^2 -alkenic region (5–7 ppm), which suggests the absence of diatropic ring current (Figure 3a). Under low-temperature NMR measurement, three sets of inner NH signals appear in the lower-field region (10–14 ppm), which suggests that there are no keto-enol tautomeric forms for **c-3a**. Several possible conformers, such as a rectangular, figure-of-eight, triangle, and dumbbell shape, can be assumed for **c-3a** (Figure S6 in the Supporting Information). With the aid of theoretical calculation, the distorted rectangular geometry can be one of the considerable structures in terms of the thermodynamic stabilization energy.⁴⁰ Critically, the ^{19}F NMR spectrum exhibits specific 3(2+1):1:2 integral patterns for the *meso*-aryl ring para-position ^{19}F atoms, providing a ready indication of the lowered molecular symmetry of the hexaphyrin core (Figure S1b in the Supporting Information). This is in sharp contrast to the spectrum of the *transoid* **t-2a**, which presents a symmetrical 2:2:2 ratio pattern for the *para*-fluorine resonances, which is normal for a rectangular structure (Figure S1c). Thus, we assumed that **c-3a** adopts a lower-symmetry structure where the inner carbonyl groups are facing in the same direction as the macrocycle.

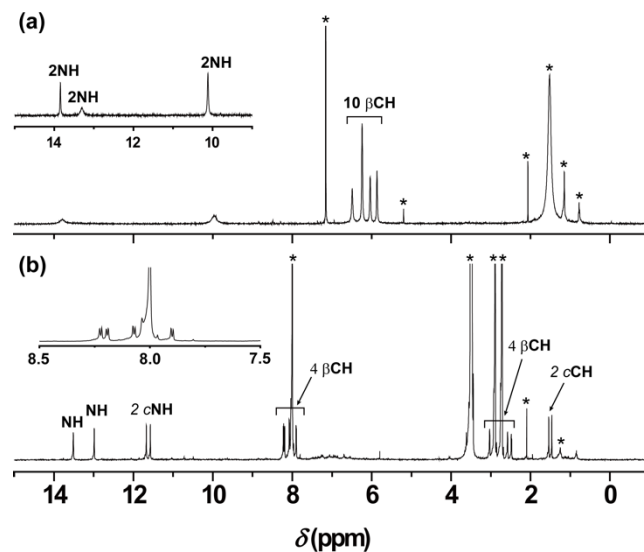


Figure 3. ^1H NMR spectra of (a) **c-3a** in CDCl_3 and (b) **c-2a** obtained upon standing in $\text{DMF-}d_7$ solution under air for 4 days. Insets are the partial spectra in CDCl_3 at 248 K and the magnified region (7.5–8.5 ppm) in $\text{DMF-}d_7$, respectively.

Effect of Solvent on the Redox-Induced Transformation into Aromatic Congeners. Typically, 28π -conjugated hexaphyrin derivatives exhibit highly flexible features dependent on their distinct conformations (e.g., rectangular or Möbius twist species).^{41,42} This solvent-dependent conformational change gives rise to topological switching in the aromaticity. The color of the solution of **c-3a** varies depending on the choice of solvent. For example, with polar solvents (e.g., DMF), bright green solutions are obtained, and a characteristic Soret band at 636 nm and Q-like bands around 900 nm emerge in the absorption spectrum (black line shown in Figure 2b). The ^1H NMR spectrum of **c-3a** recorded in $\text{DMF-}d_7$ shows an inequivalent signal pattern in the entire spectral region (–1–10 ppm) (Figure S7a). With the aid of 2D-NMR spectroscopy, absence of two NH signals implies that the species may be deprotonated because of the distinct basicity of the DMF solvent.⁴³ Deprotonation of **c-3a** by titration with *n*-tetrabutylammonium fluoride in CH_2Cl_2 resulted in a similar spectral change (Figure S9).^{44–46} Although our efforts failed to identify the accurate conformation, presumably due to the dynamic conformational behavior in solution and the facile redox reactivity (*vide infra*), the spectroscopic features indicate the formation of a dianionic Möbius-twist aromatic species, presumably (**c-3a**²⁻; eq 1).⁴⁷ This behavior is analogous to that of regular 28π hexaphyrins, which show solvent-dependent topological switching (Figure 2b).⁴⁸ Furthermore, a similar spectrum is seen using CD_3OD , suggesting the predominance of the twisted conformer with distinct aromaticity (Figure S10). In this spectrum, all the NH protons are replaced with deuterons, resulting in the appearance of ten peripheral CH signals. In $\text{THF-}d_8$ solution, the conformational interconversion is dynamic and fast as inferred from the temperature-variable absorption and ^1H NMR spectral changes (Figure S11). An averaged ^1H NMR spectral feature of a mixture of isomers, nonaromatic and postulated aromatic, was observed.

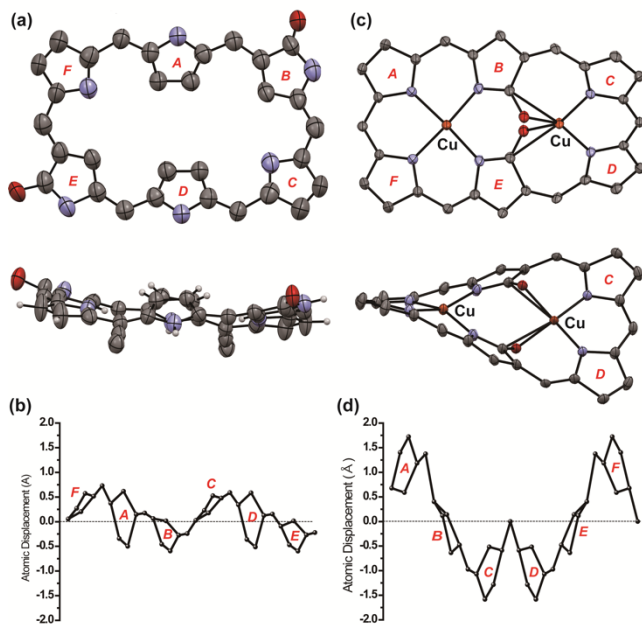
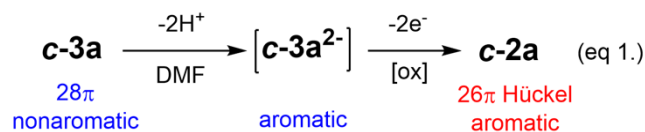


Figure 4. X-ray crystal structures of (a) **c-2b** and (c) **c-Cu₂-2a** as viewed from the top and side (50% thermal ellipsoids probabilities). The hydrogen atoms, co-crystallized solvent molecules, and *meso*-pentafluorophenyl/TIPS-ethynyl groups are omitted for clarity. Out-of-plane displacements (in units of Å) of the core atoms of (b) **c-2b** and (d) **c-Cu₂-2a** from the mean plane of 36 atoms.



Unprecedentedly, the dianionic form of the 28 π dioxohexaphyrin (**c-3a²⁻**) in DMF solution transforms into the corresponding aromatic species (i.e., **c-2a**) under ambient conditions (Scheme 1). The absorption spectrum of the **c-3a²⁻** product was measured for a solution sample after standing for 24 h and compared with the aromaticity-associated spectral signature (red line shown in Figure 2b). The change in the ¹H NMR spectrum of **c-3a²⁻** indicates the distinct conformational change, as inferred from the signal distribution; six characteristic C-H signals in the high-field region (2–4 ppm), four deshielded peripheral C-H resonances (7–9 ppm), and four NH signals in the 11–14 ppm (Figure 3b). The difference between the chemical shifts of the most shielded and deshielded hydrogen atoms ($\Delta\delta_{\text{CH-NH}}$) is estimated to be –14.88 ppm, which is attributed to the presence of a strong diamagnetic ring current in the product. Along with the inequivalent resonance pattern of the ¹⁹F NMR spectrum, a rectangular core structure was predicted, as shown in Scheme 1 (Figure S12). Evidence of the rectangular structure was provided by X-ray crystallographic analysis of the *meso*-ethynyl-substituted derivative (**c-2b**) (Figure 4a and Table S1).⁴⁹ The corresponding confused rings (B/E rings depicted in Figure 4a) are located diagonally on the opposite corners of the rectangular-shaped hexaphyrin core with outward directing amide groups.⁵⁰ The central pyrrole rings (A/D rings) are tilted by ca. 30° from the mean plane of the core, like that observed for rectangular 26 π hexaphyrins (Figure 4b).⁵¹ The co-crystallized DMF molecules interact with the outward-pointing NH moiety. The C α –N–C α bond angle of the regular C/F rings is calculated to be 100.58°. The relatively small angle indicates a preference for imino-type pyrrol-

ic structures. The harmonic oscillator model of aromaticity (HOMA) value for **c-2b** was estimated to be 0.792, indicating aromatic character.⁵² On this basis, a distinct 26 π conjugated circuit can be considered for **c-2a**, which is attributed to aerobic oxidation of the dianionic **c-3a** to the coplanar 26 π aromatic species **c-2a**.

The intrinsic chemical instability of **c-2a** was observed by removal of the DMF solvent and re-dissolving in CH₂Cl₂, which gave the original brownish-color solution. Upon passing through a short SiO₂ column, the initial 28 π species **c-3a** was recovered. Furthermore, the corresponding 26 π aromatic congener **c-2a** was not obtained by chemical oxidation with DDQ or MnO₂ in less polar solvents such as CH₂Cl₂ and toluene.

Analysis of excited-state dynamics by femtosecond time-resolved transient absorption (fs-TA) spectroscopy is a powerful tool for gaining insight into the extent of aromaticity in a material.^{53–55} The fs-TA spectrum for the Hückel-aromatic **c-2a** prepared *in situ* in DMF solution shows stronger ground-state bleaching (GSB) bands compared to the excited-state absorption (ESA) (Figure 5b). The decay time constant for **c-2a** (310 ps) is much longer than that observed in the typical 26 π Hückel-aromatic hexaphyrin **4** (98 ps) and the *transoid*-isomer **t-2a** (62 ps).^{56,57} This is in sharp contrast to the spectra obtained from toluene, which exhibit stronger ESA bands with short-lived S₁-state lifetimes for **c-3a** (τ_s = 35 ps) (Figure 5a). The emergence of emission characteristics for **c-2** in DMF (λ_{em} = 1060 nm, λ_{ex} = 635 nm) is also consistent with typical spectroscopic signature of aromatic hexaphyrins (Figure S16). The long decay component in the TA spectra of **c-2a** can be explained by intersystem crossing to the triplet state. In fact, the TA spectral data for dianionic **c-3a** (proposed to be a Möbius twist) tentatively formed in DMF show similar features, such as strong GSB bands and the longer singlet lifetime of 200 ps (Figure S16a). This aromatic diagnostic feature is likely identical to those of **c-2a** generated in DMF.

The aromatic features of **c-2a** were further investigated using density functional theory (DFT) calculations at the B3LYP/6-31G(d,p) level of theory. The molecular structure of **c-2a** resembles a regular 26 π hexaphyrin congener with rectangular geometry. In fact, the resulting coplanar geometry of **c-2a** is thermodynamically unfavorable compared with that of the *transoid*-structural isomer **t-2a** ($\Delta E_{\text{cis-trans}}$ = +26.32 kcal mol⁻¹) or another *cisoid*-isomers (e.g., $\Delta E \sim +16.8$ kcal mol⁻¹) (Figure S17a). However, the solvation (most likely hydrogen-bonding interactions between the peripheral NHs and DMF molecules) may affect stabilizing the rectangular conformer (Figure S17b).⁴¹ The frontier molecular orbitals (MOs) of **c-2a**, however, show degenerate HOMO–1/HOMO and LUMO/LUMO+1 states, following standard Gouterman's four-orbital model, like **t-2a** (Figure 6).⁴⁸ The configurational interactions between the frontier MOs result in the characteristic absorption transitions of aromatic porphyrinoids (Figure S18 and Table S2). The negative nucleus-independent chemical shift (NICS(0)) value determined at the global center of the macrocycle (–12.1 ppm) and clockwise ring current densities in the anisotropy of the induced current density (ACID) plot both indicate distinct 26 π aromaticity (Figure S19a).^{58,59} The ACID plot of **c-2a** reveals a clockwise ring current flow in the macrocyclic ring under an external magnetic field. In the case of the *transoid*-isomer **t-2a**, the core structure of the optimized structure is greatly flattened due to the intrinsic inner hydrogen-bonding network, which gives rise to the higher negative NICS(0) value of –13.8 ppm as well as remarkably strong ring current revealed by the ACID plot (Figure S19b).

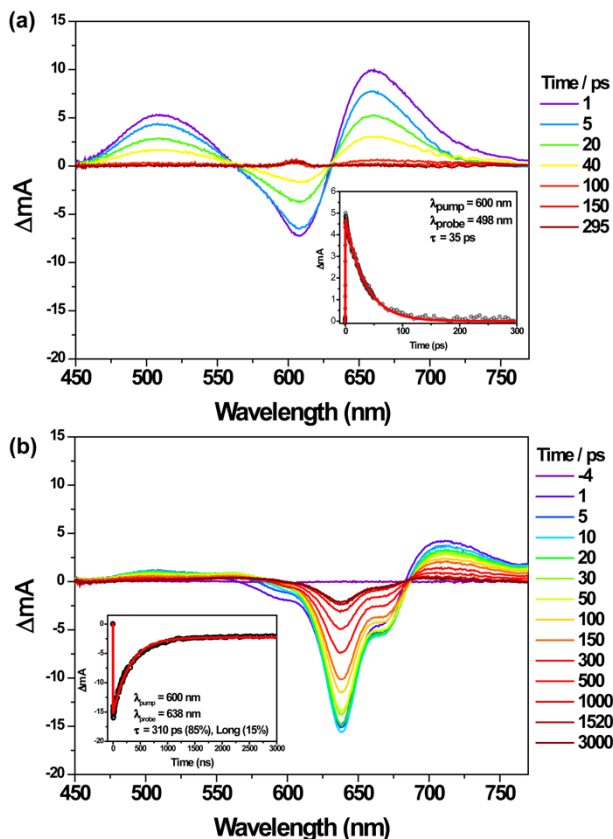


Figure 5. Femtosecond transient absorption spectra of (a) *c*-3a in toluene and (b) *c*-2a in DMF upon standing the solution in air. Insets show the decay-time profiles with least-square fitting curves.

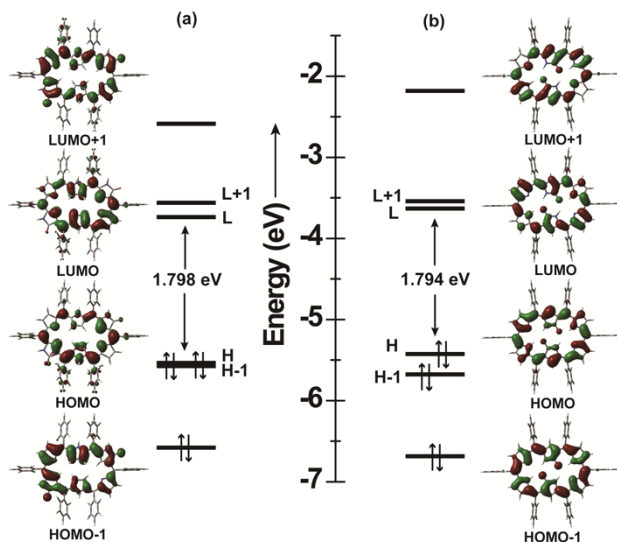


Figure 6. MO energy diagrams of (a) *c*-2a and (b) *t*-2a as derived by B3LYP/6-31G(d,p)-level DFT calculations.

Transformation into 26 π Aromatic Bis-Metal complexes. Bis-metal complexation of *c*-3a accompanied by two-electron oxidation yields 26 π aromatic dioxohexaphyrin species (Scheme 1). Treatment with either zinc(II) or copper(II) acetate salts in a CH₂Cl₂/MeOH mixed solution at room temperature resulted in the formation of bis-

metal complexes (i.e., *c*-Zn₂-2a and *c*-Cu₂-2a) in approximately quantitative yields. Interestingly, the metalation was completed in a short time (ca. 30 min) under the above conditions, which was considerably faster than that observed with *t*-2a (ca. 24 h), presumably due to the pre-organized distorted geometry of *c*-3a allowing facile metal access to the Lewis basic inner nitrogen and oxygen sites.³⁶ The solid-state geometry of bis-copper complex *c*-Cu₂-2a was unambiguously determined by X-ray crystallographic analysis (Figure 4c and Table S1). Two copper atoms are located within the porphyrin-like square planar NNNN site as well as the compressed tetrahedral NNOO one. There are no counter anions in the crystal lattice. Unlike the highly planar *t*-Cu₂-2a, the complex *c*-Cu₂-2a has a severely saddle-distorted core geometry with a large mean deviation value of 0.80 Å (Figure 4d). The HOMA value was calculated to be 0.761, reflecting weaker π -overlapping interactions. Presence of seven-membered rings at the heteroleptic NNOO copper coordination site gives rise to a distorted saddle-shape geometry, as inferred from the smaller average angles for N–Cu–O(N) at the NNOO site (148.0°) than that of N–Cu–N at the NNNN site (158.0°). The above distorted structure of *c*-Cu₂-2a is in sharp contrast to that of *transoid t*-Cu₂-2a, which has a mean deviation value of 0.01 Å (Figure S14).³⁵ This distinct saddle-distorted core gives rise to intrinsic photophysical properties (*vide infra*).

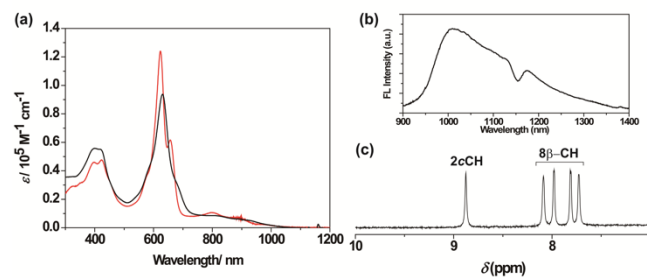


Figure 7. (a) UV-Vis-NIR absorption spectra of *c*-Zn₂-2a (red line) and *c*-Cu₂-2a (black line) in CH₂Cl₂. (b) Fluorescence spectrum of *c*-Zn₂-2a in CH₂Cl₂ upon excitation at 610 nm. (c) Partial ¹H NMR spectrum of *c*-Zn₂-2a in CD₂Cl₂ at 298 K.

In the same way, the distinct bis-zinc(II) complex *c*-Zn₂-2a shows 26 π aromatic character, as supported by the optical and NMR spectroscopic analyses. The ¹H NMR spectrum of *c*-Zn₂-2a shows five sets of β -proton signals in the typical aromatic region (δ = 8.88–7.72 ppm) at room temperature (Figures 7c and S20). When the complex was treated with an excess amount of pyridine, remarkably high-field shifted signals of the pyridines (*o*-, *m*-, *p*-CHs) bound at the Lewis acidic zinc centers of the complex (i.e., *c*-Zn₂-2a(Py)₂) were observed at δ = 4.56, 5.79, and 6.63 ppm, respectively (Figure S19a). Upon lowering the temperature to –60 °C, anisotropic spectral separation of the proton signals at 3.47 (*o*-CH), 4.43 (*o*-CH), 5.16 (*m*-CH), 5.75 (*m*-CH), 6.08 (*p*-CH), and 6.64 (*p*-CH) ppm was observed (Figure S20b). This is due to the unsymmetrical binding of the pyridines at the NNNN- and NNOO-supported zinc centers in *c*-Zn₂-2a. As revealed by the ¹H NMR spectrum of *t*-Zn₂-2a, the weaker diatropic ring current effect might be attributed to distortion of the 26 π -electron circuit.⁹ The characteristic Soret-like band at λ = 623 nm and resolved Q-like bands in the NIR region as well as an actual fluorescent emission at λ_{em} = 1010 nm indicate the aromatic signatures of the resulting dioxohexaphyrin (Figure 7a,b). The relative emission intensity is ca. five-fold smaller than that of *t*-Zn₂-2a, which is well-

agreement with a short-lived S1 excited-state lifetime for *c*-Zn₂-2a with a decay constant of $\tau_s = 220$ ps in toluene compared with that of *t*-Zn₂-2a ($\tau_s = 267$ ps) (Figure S16b).⁵⁶ Instead, the relatively long decay component arising from population of the triplet-state manifold is likely increased.

In the MO diagram of the distorted *c*-Zn₂-2a, unsymmetrical density distributions are shown along with the highly degenerate HOMO/HOMO-1 and LUMO/LUMO+1 pair. Thus, the resulting HOMO-LUMO energy gap becomes larger than that of *t*-Zn₂-2a (Figure 8).⁶⁰ The time-dependent (TD) DFT calculations indicate a distinctly lower oscillator strength (*f*) for the lowest energy transition, which is in accordance with the absorption spectra (Figure S21 and Table S3). The distortion of the core geometry does indeed cause the weak 26 π -aromatic nature as indicated by the relatively small negative NICS(0) value of -6.24 ppm for the global center of the macrocycle in *c*-Zn₂-2a compared with that in *t*-Zn₂-2a (-15.28 ppm).⁵⁹ Furthermore, the less effective connectivity of the current densities in the ACID plot support this conclusion (Figure S22).⁵⁸ However, even with this distortion, it is anticipated that the strain energy of the saddle-distorted *c*-Zn₂-2a is quite small (+0.96 kcal mol⁻¹) relative to that of *t*-Zn₂-2a. This is consistent with the fact that the skeletal flexibility of large oligopyrrolic macrocyclic systems can be exploited to tune aromaticity that is dependent on conformation.⁵

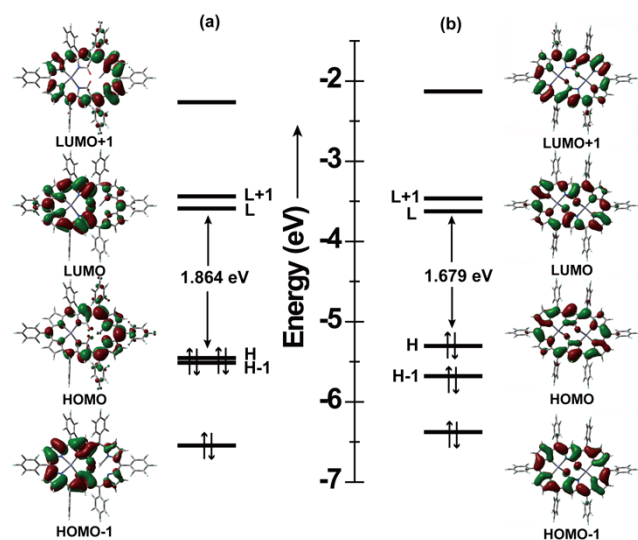


Figure 8. MO energy diagrams of (a) *c*-Zn₂-2a and (b) *t*-Zn₂-2a obtained by B3LYP/6-31G(d,p) level DFT calculations.

NIR PA Response. As observed, the *cisoid*-derivative *c*-Zn₂-2a is less emissive with a shorter excited-state lifetime than that of *transoid* *t*-Zn₂-2a (*vide supra*). We therefore evaluated the nonradiative decay of the dioxohexaphyrins using a nanosecond pulse PA measurement system.^{61,62} Due to the intrinsically low excited-state energy of the dioxohexaphyrin, the driving force for the energy transfer from the putative triplet excited state of the dioxohexaphyrin to the dioxygen should be negligible (Figure 9a). Therefore, absence of reactive oxygen species (e.g., ¹O₂) may be attributed to the extraordinarily high photostability of dioxohexaphyrins.¹⁰ For the actual production of PA (light-in/acoustic-out) signals, photostable bis-metal complexes (e.g., *c*-M₂-2a and *t*-M₂-2a) with NIR absorptions and low fluorescence quantum yields ($\Phi_{FL} < 0.001$) should be suitable as PA contrast dyes

(detailed experimental procedures are given in the Supporting Information).

Upon nanosecond pulsed laser irradiation of a DMF solution of *c*-Zn₂-2a, actual acoustic waves from the dye were detected using a piezoelectric transducer (Figure 9c). The resulting PA spectra of *c*-Zn₂-2a reveal the relatively intense PA signals in the NIR energy region (beyond 800 nm). Interestingly, the overall PA spectral features reflect the absorption spectrum. This result indicates that the intrinsic absorption profile (i.e., absorption coefficient, ϵ) of the dioxohexaphyrin-based dye governs the PA response. Excellent correlation linearity is observed for the concentration of the sample solution vs. PA intensity (Figure S23). The PA spectrum for the non-fluorescent bis-copper complex *c*-Cu₂-2a, the maximum intensity was found to be almost identical to that of emissive *c*-Zn₂-2a (Figure 9d). The measurements were conducted at the same concentration (1 mM) and laser power fluence, and the absorption coefficient value and quantum yield of nonradiative decay (Φ_{nr} ; ca. 1) for both samples are quasi-similar. Therefore, Gr \ddot{u} neisen coefficient (Γ) value may govern the PA response for *c*-M₂-2a.⁶¹

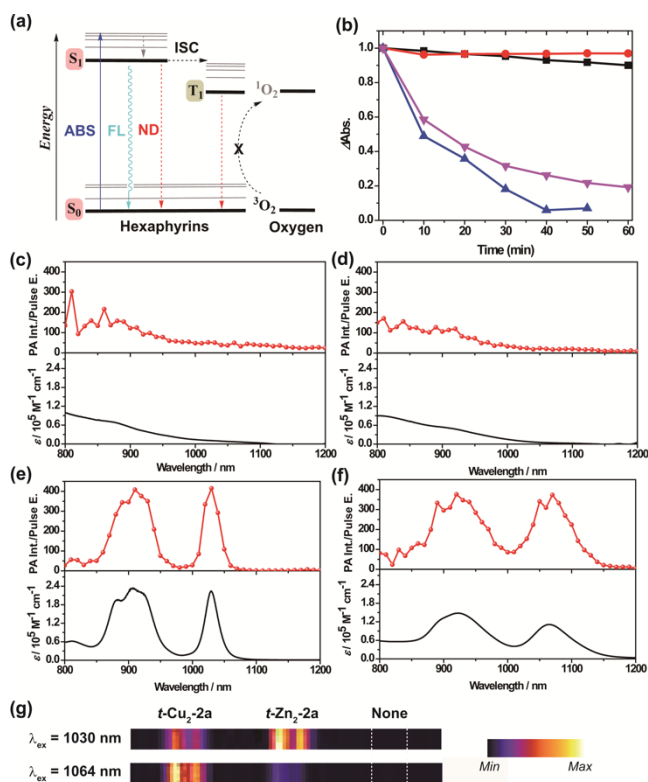


Figure 9. (a) Schematic of the photoexcitation decay process of the metallohexaphyrins; ABS, absorption; FL, fluorescence; ND, nonradiative decay. (b) Time courses of absorption changes at certain energies for *t*-Zn₂-2a (black), *t*-Cu₂-2a (red), IR-26 (blue), and IR-1040 (purple) upon laser irradiation at 1064 nm. NIR PA spectra of (c) *c*-Zn₂-2a, (d) *c*-Cu₂-2a, (e) *t*-Zn₂-2a, and (f) *t*-Cu₂-2a in DMF (top) along with the steady-state absorption spectra (bottom). (g) PA images (probed at 1030 and 1064 nm) of *t*-Cu₂-2a and *t*-Zn₂-2a in a glass-capillary (dimensions = 20 mm \times 1 mm) in comparison with a blank solvent (DMF). Concentration of sample solution is 1 mM.

Clearly, the PA properties of *transoid* bis-metal complexes are remarkable, with higher responses in the NIR-II region (Figures 9e,f and S23). The relative intensity factors of the PA signal (from the DMF solution excited at 760 nm) for the *transoid t-Zn₂-2a* and *t-Cu₂-2a* are estimated to be 1.2- and 1.4-fold higher, respectively, compared with those of freebase *t-2a* (Figure S24). This implies that the metal-coordination of *t-2a* enhances the PA signal intensity. The PA response for *t-M₂-2a* is further higher than those of commercially available indocyanine green (ICG; 2.5–2.9-fold) and regular hexaphyrin **4** (1.3–1.5-fold), respectively (Figure S24). Different with the *cisoid*-derivative system, the Γ factor may be apparently higher for non-emissive *t-Cu₂-2a* than emissive *t-Zn₂-2a* with a large absorption coefficient, which affords a relatively large PA signal.⁵⁶ Due to the inherent molecular orbital interaction, the *transoid t-Cu₂-2a* showed broader PA spectral feature, which could be advantageous to effective photo-excitation of the dye (Figure S25). The result indicates the electronic tunability of the PA properties for *transoid*-dioxohexaphyrin dyes through metal complexation.

Importantly, the extraordinarily high photostability of the dioxohexaphyrin dyes compared to those of commercially available NIR-II dyes, i.e., IR-26 and IR-1040, should be advantageous for deep PA imaging applications in terms of MPE (Figures 9b and S26). Furthermore, the PA images obtained by employing *t-Cu₂-2a* and *t-Zn₂-2a* as NIR-II PA dyes reveal the wavelength-dependent signal response in the NIR-II region, whereas no signals are generated by the blank solution (Figure 9g). Although further studies on the structure-PA property relationships are needed, these dioxohexaphyrin-based dyes can be a new entry to the NIR-II PA imaging agents.

CONCLUSIONS

In summary, we have presented a novel core-modification for controlling the molecular geometries of dioxohexaphyrin scaffolds. This strategy allowed us to distinguish strongly aromatic *transoid*- and nonaromatic *cisoid*-dioxohexaphyrin homologs, *t-2* and *c-3*, respectively. The latter 28 π -conjugated species demonstrated unique redox reactivity, interconverting to the 26 π Hückel-aromatic congeners *c-2* and *c-M₂-2* upon solvent-assisted oxidation and bis-metalation-induced oxidation, respectively. The new *cisoid*-homologs possessing two carbonyl groups within the same cavity (*c-M₂-2*) have a saddle-distorted π -conjugated circuit with moderate aromaticity. The core distortion of bis-metal complexes was reflected in the alteration of their photophysical properties, that is, broader NIR absorption, weaker emission, shorter excited-state lifetimes, and lower photoacoustic response. In contrast, the *transoid*-dioxohexaphyrin *t-2a* possessing two symmetrical “NNNO” coordination spheres afforded the corresponding bis-metal complexes *t-M₂-2a* with extraordinary photostability and intense NIR-II absorption/emission/PA signals owing to their distinctly aromatic electronic structures.

Although several porphyrin-based PA dyes have been reported, our metallo-dioxohexaphyrin dyes may be the first small molecule-based PA agents that respond to NIR-II light excitation (particularly at 1064 nm by commonly available Nd:YAG lasers). The photophysical properties can be easily tuned by metal coordination. Thus, these hexaphyrin-related molecules constitute a promising platform for deep-tissue NIR-II PA imaging applications with high spatial resolution as well as photothermal (PT) therapy.⁶⁴

ASSOCIATED CONTENT

Supporting Information

The Supporting Information is available free of charge on the ACS Publications website at DOI: 10.1021/jacs.xxxxxx.

Full experimental methods including detailed synthetic procedures, synthesis and characterization data, NMR, FAB MS, spectroscopic data, X-ray crystallographic details, and DFT calculations (PDF)

Crystallographic data for *c-Cu₂-2a* (CIF)

Crystallographic data for *c-2b* (CIF)

AUTHOR INFORMATION

Corresponding Author

*ishida.masatoshi.686@m.kyushu-u.ac.jp

*dongho@yonsei.ac.kr

*hfuruta@cstf.kyushu-u.ac.jp

ORCID

Shigeki Mori: 0000-0001-6731-2357

Koji Miki: 0000-0002-4670-2302

Kouichi Ohe: 0000-0001-8893-8893

Masatoshi Ishida: 0000-0002-1117-2188

Dongho Kim: 0000-0001-8668-2644

Hiroyuki Furuta: 0000-0002-3881-8807

Notes

The authors declare no competing financial interest.

ACKNOWLEDGMENTS

The present work at Kyushu University was supported by JSPS KAKENHI Grant Numbers (JP19H04586 and JP19K05439). Funding from the Tokuyama Research Foundation is gratefully acknowledged. The work at Yonsei University was supported by the Strategic Research (NRF2016R1E1A1A01943379) through the National Research Foundation of Korea (NRF) funded by the Ministry of Science.

REFERENCES

- Osuka, A.; Saito, S. Expanded Porphyrins and Aromaticity. *Chem. Commun.* **2011**, *47*, 4330–4339.
- Tanaka, T.; Osuka, A. Chemistry of *Meso*-Aryl-Substituted Expanded Porphyrins: Aromaticity and Molecular Twist. *Chem. Rev.* **2017**, *117*, 2584–2640.
- Roznyatovskiy, V. V.; Lee, C. H.; Sessler, J. L. π -Extended Isomeric and Expanded Porphyrins. *Chem. Soc. Rev.* **2013**, *42*, 1921–1933.
- Sessler, J. L.; Seidel, D. Synthetic Expanded Porphyrin Chemistry. *Angew. Chem., Int. Ed.* **2003**, *42*, 5134–5175.
- Szyszkowski, B.; Biłek, M. J.; Pacholska-Dudziak, E.; Latos-Grazyński, L. Flexible Porphyrinoids. *Chem. Rev.* **2017**, *117*, 2839–2909.
- Saito, S.; Osuka, A. Expanded Porphyrins: Intriguing Structures, Electronic Properties, and Reactivities. *Angew. Chem., Int. Ed.* **2011**, *50*, 4342–4373.
- Alka, A.; Shetti, V. S.; Ravikanth, M. Coordination Chemistry of Expanded Porphyrins. *Coord. Chem. Rev.* **2019**, *401*, 213063.

- (8) Zhu, X. J.; Fu, S. T.; Wong, W. K.; Guo, J. P.; Wong, W. Y. A Near-Infrared-Fluorescent Chemodosimeter for Mercuric Ion Based on an Expanded Porphyrin. *Angew. Chem., Int. Ed.* **2006**, *45*, 3150–3154.
- (9) Ikawa, Y.; Takeda, M.; Suzuki, M.; Osuka, A.; Furuta, H. Water-Soluble Doubly N-Confused Hexaphyrin: A Near-IR Fluorescent Zn(II) Ion Sensor in Water. *Chem. Commun.* **2010**, *46*, 5689–5691.
- (10) Higashino, T.; Nakatsuji, H.; Fukuda, R.; Okamoto, H.; Imai, H.; Matsuda, T.; Tochio, H.; Shirakawa, M.; Tkachenko, N. V.; Hashida, M.; Murakami, T.; Imahori, H. Hexaphyrin as a Potential Theranostic Dye for Photothermal Therapy and ^{19}F Magnetic Resonance Imaging. *ChemBioChem* **2017**, *18*, 951–959.
- (11) Tian, J.; Ding, L.; Xu, H. J.; Shen, Z.; Ju, H.; Jia, L.; Bao, L.; Yu, J. S. Cell-Specific and pH-Activatable Rubyryin-Loaded Nanoparticles for Highly Selective Near-Infrared Photodynamic Therapy against Cancer. *J. Am. Chem. Soc.* **2013**, *135*, 18850–18858.
- (12) Tanaka, T.; Sugita, T.; Tokuji, S.; Saito, S.; Osuka, A. Metal Complexes of Chiral Möbius Aromatic [28]Hexaphyrin(1.1.1.1.1.1): Enantiomeric Separation, Absolute Stereochemistry, and Asymmetric Synthesis. *Angew. Chem., Int. Ed.* **2010**, *49*, 6619–6621.
- (13) Ruffin, H.; Boussambe, G. N. M.; Roisnel, T.; Dorcet, V.; Boitrel, B.; Le Gac, S. Tren-Capped Hexaphyrin Zinc Complexes: Interplaying Molecular Recognition, Möbius Aromaticity, and Chirality. *J. Am. Chem. Soc.* **2017**, *139*, 13847–13857.
- (14) Benchouaia, R.; Cissé, N.; Boitrel, B.; Sollogoub, M.; Le Gac, S.; Ménand, M. Orchestrating Communications in a Three-Type Chirality Totem: Remote Control of the Chiroptical Response of a Möbius Aromatic System. *J. Am. Chem. Soc.* **2019**, *141*, 11583–11593.
- (15) Szyszko, B.; Przewoźnik, M.; Bialek, M. J.; Białońska, A.; Chmielewski, P. J.; Cichos, J.; Latos-Grażyński, L. Helicenophyrins: Expanded Carbaporphyrins Incorporating Aza[5]helicene and Heptacyclic S-Shaped Aza[5]helicene Motifs. *Angew. Chem., Int. Ed.* **2018**, *57*, 4030–4034.
- (16) Blusch, L. K.; Hemberger, Y.; Pröpper, K.; Dittrich, B.; Witterauf, F.; John, M.; Bringmann, G.; Brückner, C.; Meyer, F. Siamese-Twin Porphyrin: A Pyrazole-Based Expanded Porphyrin of Persistent Helical Conformation. *Chem. – A Eur. J.* **2013**, *19*, 5868–5880.
- (17) Ge, X.; Fu, Q.; Bai, L.; Chen, B.; Wang, R.; Gao, S.; Song, J. Photoacoustic Imaging and Photothermal Therapy in the Second Near-Infrared Window. *New J. Chem.* **2019**, *43*, 8835–8851.
- (18) Huang, K.; Zhang, Y.; Lin, J.; Huang, P. Nanomaterials for Photoacoustic Imaging in the Second Near-Infrared Window. *Biomater. Sci.* **2019**, *7*, 472–479.
- (19) Upputuri, P. K.; Pramanik, M. Photoacoustic Imaging in the Second Near-Infrared Window: A Review. *J. Biomed. Opt.* **2019**, *24*, 040901.
- (20) American National Standard Institute. American National Standard for Safe Use of Lasers (ANSI Z136.1-2014). *Am. Natl. Stand. Institute, Inc.* **2014**.
- (21) Smith, A. M.; Mancini, M. C.; Nie, S. Second Window for in Vivo Imaging. *Nat. Nanotechnol.* **2009**, *4*, 710–711.
- (22) Hong, G.; Antaris, A. L.; Dai, H. Near-Infrared Fluorophores for Biomedical Imaging. *Nat. Biomed. Eng.* **2017**, *1*, 10.
- (23) Okumura, K.; Yoshida, K.; Yoshioka, K.; Aki, S.; Yoneda, N.; Inoue, D.; Kitao, A.; Ogi, T.; Kozaka, K.; Minami, T.; Koda, W.; Kobayashi, S.; Takuwa, Y.; Gabata, T. Photoacoustic Imaging of Tumour Vascular Permeability with Indocyanine Green in a Mouse Model. *Eur. Radiol. Exp.* **2018**, *2*, 5.
- (24) Zhou, E. Y.; Knox, H. J.; Liu, C.; Zhao, W.; Chan, J. A Conformationally Restricted Aza-BODIPY Platform for Stimulus-Responsive Probes with Enhanced Photoacoustic Properties. *J. Am. Chem. Soc.* **2019**, *141*, 17601–17609.
- (25) Gawale, Y.; Adarsh, N.; Kalva, S. K.; Joseph, J.; Pramanik, M.; Ramaiah, D.; Sekar, N. Carbazole-Linked Near-Infrared Aza-BODIPY Dyes as Triplet Sensitizers and Photoacoustic Contrast Agents for Deep-Tissue Imaging. *Chem. – A Eur. J.* **2017**, *23*, 6570–6578.
- (26) Liu, S.; Zhou, X.; Zhang, H.; Ou, H.; Lam, J. W. Y.; Liu, Y.; Shi, L.; Ding, D.; Tang, B. Z. Molecular Motion in Aggregates: Manipulating TICT for Boosting Photothermal Theranostics. *J. Am. Chem. Soc.* **2019**, *141*, 5359–5368.
- (27) Sun, Y.; Ding, F.; Zhou, Z.; Li, C.; Pu, M.; Xu, Y.; Zhan, Y.; Lu, X.; Li, H.; Yang, G.; Sun, Y.; Stang, P. J. Rhomboidal Pt(II) Metallacycle-Based NIR-II Theranostic Nanoprobe for Tumor Diagnosis and Image-Guided Therapy. *Proc. Natl. Acad. Sci. U. S. A.* **2019**, *116*, 1968–1973.
- (28) Toriumi, N.; Asano, N.; Ikeno, T.; Muranaka, A.; Hanaoka, K.; Urano, Y.; Uchiyama, M. Design of Photostable, Activatable Near-Infrared Photoacoustic Probes Using Tautomeric Benzophthalocyanine as a Platform. *Angew. Chem., Int. Ed.* **2019**, *58*, 7788–7791.
- (29) Ho, I. T.; Sessler, J. L.; Gambhir, S. S.; Jokerst, J. V. Parts per Billion Detection of Uranium with a Porphyrinoid-Containing Nanoparticle and in Vivo Photoacoustic Imaging. *Analyst* **2015**, *140*, 3731–3737.
- (30) Ho, I.-T.; Zhang, Z.; Ishida, M.; Lynch, V. M.; Cha, W.-Y.; Sung, Y. M.; Kim, D.; Sessler, J. L. A Hybrid Macrocyclic with a Pyridine Subunit Displays Aromatic Character upon Uranyl Cation Complexation. *J. Am. Chem. Soc.* **2014**, *136*, 4281–4286.
- (31) Zhou, Y.; Wang, D.; Zhang, Y.; Chitgupi, U.; Geng, J.; Wang, Y.; Zhang, Y.; Cook, T. R.; Xia, J.; Lovell, J. F. A Phosphorus Phthalocyanine Formulation with Intense Absorbance at 1000 Nm for Deep Optical Imaging. *Theranostics* **2016**, *6*, 688–697.
- (32) Furuyama, T.; Satoh, K.; Kushiya, T.; Kobayashi, N. Design, Synthesis, and Properties of Phthalocyanine Complexes with Main-Group Elements Showing Main Absorption and Fluorescence beyond 1000 nm. *J. Am. Chem. Soc.* **2014**, *136*, 765–776.
- (33) Toganoh, M.; Furuta, H. Blooming of Confused Porphyrinoids - Fusion, Expansion, Contraction, and More Confusion. *Chem. Commun.* **2012**, *48*, 937–954.
- (34) Lash, T. D. Carbaporphyrinoid Systems. *Chem. Rev.* **2017**, *117*, 2313–2446.
- (35) Suzuki, M.; Yoon, M. C.; Kim, D. Y.; Kwon, J. H.; Furuta, H.; Kim, D.; Osuka, A. A New Entry to Doubly N-Confused [26]Hexaphyrins(1.1.1.1.1.1) from Normal [26]Hexaphyrins(1.1.1.1.1.1) through an Unprecedented Double Pyrrolic Rearrangement. *Chem. – A Eur. J.* **2006**, *12*, 1754–1759.
- (36) Srinivasan, A.; Ishizuka, T.; Osuka, A.; Furuta, H. Doubly N-Confused Hexaphyrin: A Novel Aromatic Expanded Porphyrin That Complexes Bis-Metals in the Core. *J. Am. Chem. Soc.* **2003**, *125*, 878–879.
- (37) Won, D. H.; Toganoh, M.; Terada, Y.; Fukatsu, S.; Uno, H.; Furuta, H. Near-Infrared Emission from Bis-Pt^{II} Complexes of Doubly N-Confused Calix[6]phyrins(1.1.1.1.1.1). *Angew. Chem., Int. Ed.* **2008**, *47*, 5438–5441.

- (38) Pushpanandan, P.; Won, D.-H.; Mori, S.; Yasutake, Y.; Fukatsu, S.; Ishida, M.; Furuta, H. Doubly N-Confused Calix[6]phyrin Bis-Organopalladium Complexes: Photostable Triplet Sensitizers for Singlet Oxygen Generation. *Chem. Asian J.* **2019**, *14*, 1729–1736.
- (39) Fukuzumi, S.; Honda, T.; Kojima, T. Structures and Photoinduced Electron Transfer of Protonated Complexes of Porphyrins and Metallophthalocyanines. *Coord. Chem. Rev.* **2012**, *256*, 2488–2502.
- (40) Based on the NMR spectral feature, figure-of-eight structures of **c-3a** formed in the CHCl₃ solution are also considerable. Although the relative energy for the postulated conformer B (Figure S6 in SI) was not obtained by our calculation, the distribution of the speculated chemical shift values of β-Hs for the rectangular C is likely consistent with the experimental spectrum.
- (41) Sankar, J.; Mori, S.; Saito, S.; Rath, H.; Suzuki, M.; Inokuma, Y.; Shinokubo, H.; Kil, S. K.; Zin, S. Y.; Shin, J.-Y.; Lim, J. M.; Matsuzaki, Y.; Matsushita, O.; Muranaka, A.; Kobayashi, N.; Kim, D.; Osuka, A. Unambiguous Identification of Möbius Aromaticity for Meso-Aryl-Substituted [28]Hexaphyrins(1.1.1.1.1.1). *J. Am. Chem. Soc.* **2008**, *130*, 13568–13579.
- (42) Kim, K. S.; Yoon, Z. S.; Ricks, A. B.; Shin, J.-Y.; Mori, S.; Sankar, J.; Saito, S.; Jung, Y. M.; Wasielewski, M. R.; Osuka, A.; Kim, D. Temperature-Dependent Conformational Change of *meso*-Hexakis(pentafluorophenyl) [28]Hexaphyrins(1.1.1.1.1.1) into Möbius Structures. *J. Phys. Chem. A* **2009**, *113*, 4498–4506.
- (43) Kolthoff, I. M.; Chantooni, M. K.; Smagowski, H. Acid-Base Strength in *N,N*-Dimethylformamide. *Anal. Chem.* **1970**, *42*, 1622–1628.
- (44) Cha, W. Y.; Yoneda, T.; Lee, S.; Lim, J. M.; Osuka, A.; Kim, D. Deprotonation Induced Formation of Möbius Aromatic [32]Heptaphyrins. *Chem. Commun.* **2014**, *50*, 548–550.
- (45) Cha, W. Y.; Soya, T.; Tanaka, T.; Mori, H.; Hong, Y.; Lee, S.; Park, K. H.; Osuka, A.; Kim, D. Multifaceted [36]Octaphyrin(1.1.1.1.1.1.1.1): Deprotonation-Induced Switching among Nonaromatic, Möbius Aromatic, and Hückel Antiaromatic Species. *Chem. Commun.* **2016**, *52*, 6076–6078.
- (46) Kim, J. O.; Hong, Y.; Kim, T.; Cha, W. Y.; Yoneda, T.; Soya, T.; Osuka, A.; Kim, D. Near-Infrared S₂ Fluorescence from Deprotonated Möbius Aromatic [32]Heptaphyrin. *J. Phys. Chem. Lett.* **2018**, *9*, 4527–4531.
- (47) The other conformers including the distorted triangle shape can be also considered to represent aromatic isomers. A further structural analysis of the aromatic species tentatively formed in the solution is need to reveal the dynamic behaviour of **c-2a** in solution.
- (48) Shin, J.-Y.; Kim, K. S.; Yoon, M. C.; Lim, J. M.; Yoon, Z. S.; Osuka, A.; Kim, D. Aromaticity and Photophysical Properties of Various Topology-Controlled Expanded Porphyrins. *Chem. Soc. Rev.* **2010**, *39*, 2751–2767.
- (49) This *meso*-ethynyl substituted derivative (**c-2b**) was prepared by the similar reaction procedure for the purpose of crystallographic analysis. The detailed physicochemical properties will be reported.
- (50) Mallick, A.; Oh, J.; Kim, D.; Ishida, M.; Furuta, H.; Rath, H. Induced Correspondence of a Local π-Aromatic Sextet in Heteroannulenes: Synthesis and Characterization. *Chem. – A Eur. J.* **2016**, *22*, 5504–5508.
- (51) Maria, G. P. M. S. N.; Rosalia, M. M.; Augsuto, C. T.; Armando, J. D. S.; Artur, M. S. S.; Vitor, F.; Michael, G. B. D.; Jose, A. S. C. *Meso*-Substituted Expanded Porphyrins : New and Stable Hexaphyrins. *Chem. Commun.* **1999**, 385–386.
- (52) Krygowski, T. M.; Cyrański, M. K. Structural Aspects of Aromaticity. *Chem. Rev.* **2001**, *101*, 1385–1419.
- (53) Cho, S.; Yoon, Z. S.; Kim, K. S.; Yoon, M. C.; Cho, D. G.; Sessler, J. L.; Kim, D. Defining Spectroscopic Features of Heteroannulenic Antiaromatic Porphyrinoids. *J. Phys. Chem. Lett.* **2010**, *1*, 895–900.
- (54) Yoon, M. C.; Cho, S.; Suzuki, M.; Osuka, A.; Kim, D. Aromatic versus Antiaromatic Effect on Photophysical Properties of Conformationally Locked Trans-Vinylene-Bridged Hexaphyrins. *J. Am. Chem. Soc.* **2009**, *131*, 7360–7367.
- (55) Sung, Y. M.; Oh, J.; Cha, W. Y.; Kim, W.; Lim, J. M.; Yoon, M. C.; Kim, D. Control and Switching of Aromaticity in Various All-Aza-Expanded Porphyrins: Spectroscopic and Theoretical Analyses. *Chem. Rev.* **2017**, *117*, 2257–2312.
- (56) Kim, D.; Kwon, J. H.; Ahn, T. K.; Yoon, M. C.; Kim, D. Y.; Koh, M. K.; Furuta, H.; Suzuki, M.; Osuka, A. Comparative Photophysical Properties of Free-Base, Bis-Zn(II), Bis-Cu(II), and Bis-Co(II) Doubly N-Confused Hexaphyrins(1.1.1.1.1.1). *J. Phys. Chem. B* **2006**, *110*, 11683–11690.
- (57) Ahn, T. K.; Kwon, J. H.; Kim, D. Y.; Cho, D. W.; Jeong, D. H.; Kim, S. K.; Suzuki, M.; Shimizu, S.; Osuka, A.; Kim, D. Comparative Photophysics of [26]- and [28]Hexaphyrins(1.1.1.1.1.1): Large Two-Photon Absorption Cross Section of Aromatic [26]Hexaphyrins(1.1.1.1.1.1). *J. Am. Chem. Soc.* **2005**, *127*, 12856–12861.
- (58) Geuenich, D.; Hess, K.; Köhler, F.; Herges, R. Anisotropy of the Induced Current Density (ACID), a General Method to Quantify and Visualize Electronic Delocalization. *Chem. Rev.* **2005**, *105*, 3758–3772.
- (59) Schleyer, P. V. R.; Maerker, C.; Dransfeld, A.; Jiao, H.; Van Eikema Hommes, N. J. R. Nucleus-Independent Chemical Shifts: A Simple and Efficient Aromaticity Probe. *J. Am. Chem. Soc.* **1996**, *118*, 6317–6318.
- (60) Mack, J. Expanded, Contracted, and Isomeric Porphyrins: Theoretical Aspects. *Chem. Rev.* **2017**, *117*, 3444–3478.
- (61) Lemaster, J. E.; Jokerst, J. V. What Is New in Nanoparticle-Based Photoacoustic Imaging? *Wiley Interdiscip. Rev. Nanomed. Nanobiotechnol.* **2017**, *9*, 1–11.
- (62) Lovell, J. F.; Jin, C. S.; Huynh, E.; Jin, H.; Kim, C.; Rubinstein, J. L.; Chan, W. C. W.; Cao, W.; Wang, L. V.; Zheng, G. Porphysome Nanovesicles Generated by Porphyrin Bilayers for Use as Multimodal Biophotonic Contrast Agents. *Nat. Mater.* **2011**, *10*, 324–332.
- (63) Yao, D.-K.; Zhang, C.; Maslov, K. I.; Wang, L. V. Photoacoustic Measurement of the Grüneisen Parameter of Tissue. *J. Biomed. Opt.* **2014**, *19*, 017007.
- (64) Jung, H. S.; Verwilt, P.; Sharma, A.; Shin, J.; Sessler, J. L.; Kim, J. S., Organic molecule-based photothermal agents: an expanding photothermal therapy universe. *Chem. Soc. Rev.* **2018**, *47*, 2280–2297.

SYNOPSIS TOC

Bis-Metal Complexes of Doubly N-Confused Dioxohexaphyrins as Potential Near Infrared-II Photoacoustic Dyes

Keito Shimomura,[†] Hiroto Kai,[†] Yuma Nakamura,[†] Yongseok Hong,[‡] Shigeki Mori,[§] Koji Miki,[⊥] Kouichi Ohe,[⊥] Yusuke Notsuka,[⊥] Yoshihisa Yamaoka,[⊥] Masatoshi Ishida,^{*,†} Dongho Kim,^{*,‡} and Hiroyuki Furuta^{*,†}

